An ultra-wideband pattern reconfigurable antenna based on graphene coating*

YanNan Jiang(姜彦南)[1,2,3], Rui Yuan(袁锐)[1], Xi Gao(高喜)[1,2], Jiao Wang(王娇)[1,2,3,†], SiMin Li(李思敏)[2], and Yi-Yu Lin(林诒玉)[1,2]

[1] *Guangxi Key Laboratory of Wireless Wideband Communication and Signal Processing, Guilin* 541004, *China*
[2] *Key Laboratory of Cognitive Radio and Information Processing (Ministry of Education), Guilin University of Electronic Technology, Guilin* 541004, *China*
[3] *Guangxi Experiment Center of Information Science, Guilin University of Electronic Technology, Guilin* 541004, *China*

(Received 20 April 2016; revised manuscript received 19 July 2016; published online 28 September 2016)

An ultra-wideband pattern reconfigurable antenna is proposed. The antenna is a dielectric coaxial hollow monopole with a cylindrical graphene-based impedance surface coating. It consists of a graphene sheet coated onto the inner surface of a cylindrical substrate and a set of independent polysilicon DC gating pads mounted on the outside of the cylindrical substrate. By changing the DC bias voltages to the different gating pads, the surface impedance of the graphene coating can be freely controlled. Due to the tunability of graphene's surface impedance, the radiation pattern of the proposed antenna can be reconfigured. A transmission line method is used to illustrate the physical mechanism of the proposed antenna. The results show that the proposed antenna can reconfigure its radiation pattern in the omnidirectional mode with the relative bandwidth of 58.5% and the directional mode over the entire azimuth plane with the relative bandwidth of 67%.

Keywords: ultra-wideband pattern reconfigurable antenna, graphene, impedance surface

PACS: 84.40.Ba, 84.40.–x **DOI:** 10.1088/1674-1056/25/11/118402

1. Introduction

Graphene, which is an extraordinary material with many unique properties and superiorities, has been extensively investigated in optical, mechanical, thermal, and electrical fields,[1–3] including transparent conductors for touch screens,[4,5] flexible electronics,[6] interconnects,[7] surface plasmon polaritons (SPPs) waveguides,[8,9] phase shifters,[10] and absorbers.[11–13] Thanks to the dynamical tunability of graphene conductivity that results from its field effect by applying adequate bias electrostatic, the reconfigurable graphene-based antenna has also attracted growing attention.[14–20] In the previous efforts, graphene was applied to planar or planar array with periodic units in the design of leaky-wave antennas (LWA),[15,16] reflector antennas,[17,18] and low-profile antennas.[19,20] Graphene is usually used for antennas in two forms: 1) acting as an actual radiation part, which, however, leads to a low radiation efficiency due to the loss caused by the real part of graphene surface conductivity;[21,22] 2) being employed as a parasitic component, which enhances the radiation performance owning to diminish the loss.[23,24]

Recently, the graphene impedance surface is frequently presented to improve the performances of various antennas. These researches are mainly concentrated on THz and optical frequencies and are rarely involved in microwave range. However, with the development of art methods, large graphene flakes and graphene transferred onto flexible substrates can be produced. The technical progress makes it possible to develop graphene-based antenna with high performance in microwave frequencies.[25,26]

In the microwave band, graphene has an outstanding characteristic, i.e., the real part of the surface impedance ($R_e(Z_s) = R_e(1/\sigma_s)$) of graphene is very high without bias and becomes lower when the bias electrostatic increases. Therefore, graphene can act as a high impedance surface (HIS) on low bias electrostatic or a low impedance surface (LIS) on high bias electrostatic.[14] Moreover, the $R_e(Z_s)$ varies from a few ohms to thousands of ohms. This means that the surface resistance realizes a metal–insulator transition. These characteristics have been employed to develop some novel antennas, such as smart antennas.[14] These previous antennas, however, have obvious disadvantages of a narrow bandwidth and a limited tunable range of radiation direction, which extremely limit their practical application.

In this paper, we propose a cylindrical graphene coating (CGC) in microwave range, which is made of graphene transferred onto the inner surface of SiO_2 substrate (the relative permittivity is ε_r) and a set of independent polysilicon pads located outside the cylinder. Furthermore, we design an ultra-wideband pattern reconfigurable antenna which consists of a

*Project supported by the National Natural Science Foundation of China (Grant Nos. 61661012, 61461016, and 61361005), the Natural Science Foundation of Guangxi, China (Grant Nos. 2015GXNSFBB139003 and 2014GXNSFAA118283), Program for Innovation Research Team of Guilin University of Electromagnetic Technology, China, and the Dean Project of Guangxi Key Laboratory of Wireless Wideband Communication and Signal Processing, China.

†Corresponding author. E-mail: wangjiao@guet.edu.cn

© 2016 Chinese Physical Society and IOP Publishing Ltd

monopole and the CGC. The proposed antenna has high radiation performance in an ultra-wideband because of the characteristic of the metal–insulator transition of the graphene coating. Meanwhile, the antenna realizes directional radiation, whose direction can be continuously adjusted in the entire azimuth, or omnidirectional radiation.

The rest of this paper is arranged as follows. The surface impedance of the graphene in microwave range is presented in Section 2. In Section 3, the design of a 3D ultra-wideband pattern reconfigurable antenna with CGC is given. In order to demonstrate the ultra-wideband and reconfigurable radiation characteristics of the proposed antenna, numerical results are analyzed using the transmission line (TL) model and simulated using CST software respectively in Section 3. Finally, the conclusions are drawn in Section 4.

2. Graphene-based impedance surface in microwave band

Graphene can be regarded as an infinitesimally thin surface, whose surface conductivity σ_s in the absence of magnetostatic bias and spatial dispersion is analytically expressed using the well-known Kubo formula[27]

$$\sigma_s = \frac{\mathrm{j}e^2(\omega-\mathrm{j}2\Gamma)}{\pi\hbar^2} \times \left[\frac{1}{(\omega-\mathrm{j}2\Gamma)^2}\int_0^\infty \varepsilon\left(\frac{\partial f_d(\varepsilon)}{\partial\varepsilon}-\frac{\partial f_d(-\varepsilon)}{\partial\varepsilon}\right)\mathrm{d}\varepsilon - \int_0^\infty\left(\frac{\partial f_d(-\varepsilon)-\partial f_d(\varepsilon)}{(\omega-\mathrm{j}2\Gamma)^2-4(\varepsilon/\hbar)^2}\right)\mathrm{d}\varepsilon\right], \quad (1)$$

where ε is the energy, $\hbar$ is the reduced Planck's constant, e is the charge of an electron, $f_d(\varepsilon)=1/(\exp\{(\varepsilon-\mu_c)/k_BT\}+1)$ is the Fermi–Dirac distribution,[28] k_B is the Boltzmann's constant, and ω, μ_c, Γ, and T are the angular frequency, the chemical potential (it is determined by either an applied biasing electrostatic or chemical doping), the phenomenological scattering rate, and the temperature, respectively. In Eq. (1), the first and the second terms are called the intraband conductivity and the interband conductivity, respectively. The intraband term can be evaluated as[27]

$$\sigma_{\mathrm{intra}} = \frac{e^2k_BT/2\Gamma}{\pi\hbar^2(1+\mathrm{j}\omega/2\Gamma)}\left(\frac{\mu_c}{k_BT}+2\ln(e^{-\mu_c/k_BT}+1)\right), \quad (2)$$

and the interband term, in general, must be evaluated numerically. Now, the surface impedance of graphene is defined as

$$Z_s(E_b)=1/\sigma_s=R_s(E_b)+\mathrm{j}X_s(E_b), \quad (3)$$

where R_s and X_s are the surface resistance and the surface reactance, respectively. Assuming non-chemically doped graphene, the electrostatic E_b regulates the carrier density as $n_s=\varepsilon_r\varepsilon_0E_b/e$. Moreover, the carrier density is related to μ_c as

$$n_s=\frac{2}{\pi\hbar^2v_f^2}\int_0^\infty \varepsilon\left[f_d(\varepsilon-\mu_c)-f_d(\varepsilon+\mu_c)\right]\mathrm{d}\varepsilon. \quad (4)$$

For $T=300$ K, $\tau=0.1$ ps, $\Gamma=1/\tau$, and $v_f=9.5\times10^5$ m/s, we obtain the surface impedance of graphene depending on frequency from Eqs. (1)–(4) by changing the biased electrostatic, as shown in Fig. 1. One can obtain the following conclusions. 1) The intraband contribution is dominant, which means that the interband term can be neglected. 2) The real part of the surface impedance remains approximately constant and is far larger than the image part. This means that the surface reactance can also be ignored. 3) The surface impedance becomes lower with the biasing electrostatic increasing and the real part varies from thousands of ohms to a few ohms. This causes the surface resistance metal–insulator transition of the surface resistance. Therefore, a reconfigurable antenna can be constructed by adjusting the graphene's metal–insulator transition, which is tuned by the biased electrostatic.

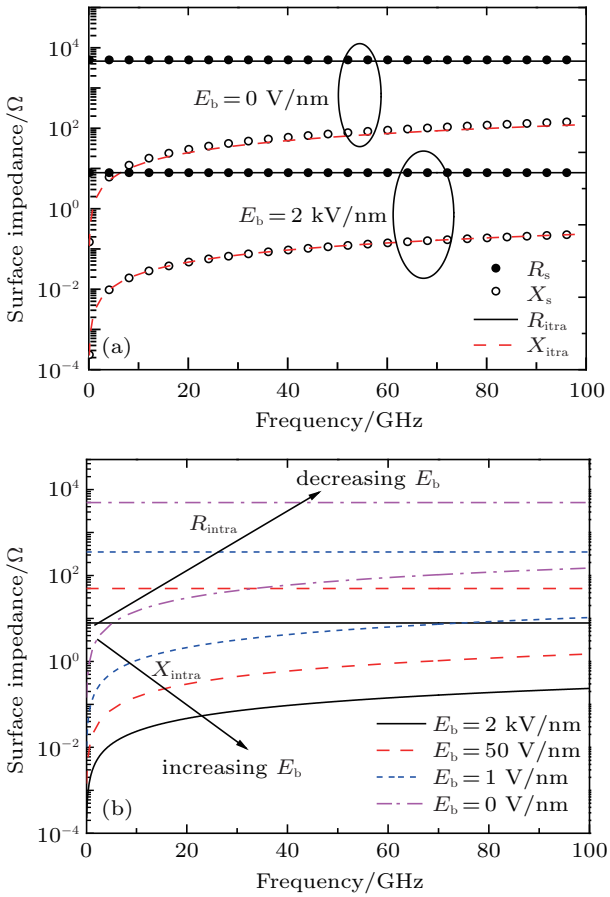


Fig. 1. (color online) Frequency dependence of graphene parameters. (a) Total and intraband term of surface resistance and surface reactance. (b) Surface resistance and surface reactance of intraband term for different E_b.

3. A 3D ultra-wideband pattern reconfigurable antenna with CGC

The configuration of the proposed antenna and its front-penetrative view are shown in Figs. 2(a) and 2(b), respectively. The number N of the polysilicon pads is set to be 36 and each polysilicon pad is labeled with an integer i ($1\le i\le 36$) the

graphene sheet is then correspondingly divided into 36 subdomains and each subdomain is also labeled with i. Throughout this study, the order of i in the Cartesian coordinate system remains unchanged, as shown in Fig. 2(b). It is well known that the bias electrostatic E_{bi} is decided by the applied DC voltage V_{DCi}, and furthermore the surface impedance for the i-th subdomain of the cylindrical graphene-based coating is controlled by the bias electrostatic E_{bi} (see Eq. (3)). Therefore, we can control the surface impedance of graphene for each subdomain by changing the DC voltage V_{DCi} freely.

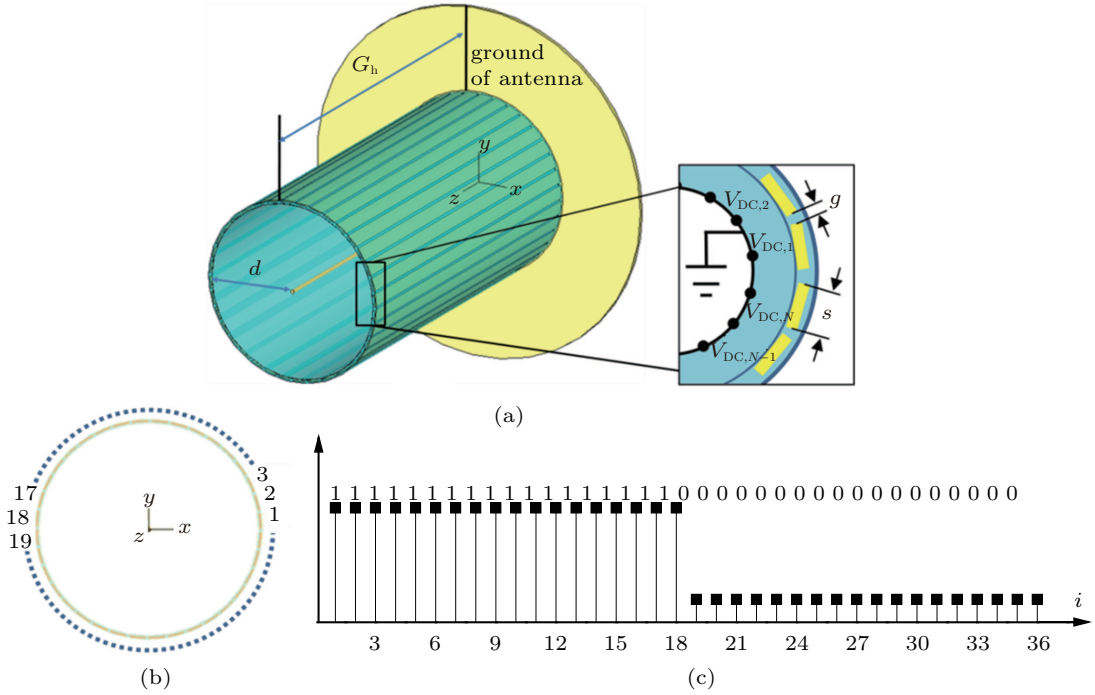


Fig. 2. (a) The proposed reconfigurable antenna using a CGC with the radius of d, (b) the front-penetrative view of the proposed configuration, and (c) an example of the binary code. The polysilicon pads (yellow in the insert) are used to control the graphene conductivity σ_s as a function of the bias electrostatic by applied DC voltage V_{DCi}. All dimensions are in millimeters: $G_h = 20$, the length l of the monopole and its ground diameter are 4.5 and 40, respectively. The distance between the pads satisfies $g << s$. The polysilicon pads and the SiO_2 substrate (with the thickness of t) are excluded in the subsequent simulation because of their extremely thin profile.[16]

In the fabrication of the proposed antenna, 36 pairs of wires can be used to bias the graphene. The two terminations of one end of each pair insert into a small hole on the ground of the antenna near the coating and connect the graphene and pad by conductive silver paste, and these of the other end connect the DC power. It is obvious that the variohm should be joined between graphene and the DC power to change the DC voltage and bias the corresponding subdomain graphene. It is worth pointing out that 1) 36 variohms are needed, 2) these variohms should be placed in the back of the antenna's ground, and 3) the electric potentials of all the terminations connecting graphene are equal. Therefore, the loss effect of the wire can be neglected if all the wires in the front of the antenna's ground are very short.

In this work, we will use two states: 1) LIS with a smaller surface impedance for the graphene with a relative high bias electrostatic; and 2) HIS with a larger surface impedance for the graphene with a low bias electrostatic. For convenience in following description, the LIS and the HIS are denoted by binary codes "1" and "0", respectively. As shown in Fig. 2(c), for example, the case of the subdomains from 1st to 18th being LIS and the rest being HIS is coded as $\underbrace{1\ldots1}_{18}\underbrace{0\ldots0}_{18}$

3.1. The ultra-wideband impedance characteristics of the proposed antenna

The TL method and the *ABCD* transmission matrices are used to analyze the ultra-wideband impedance characteristics of the proposed antenna. As shown in Fig. 2(a), when the monopole is loaded by an excitation source, the electromagnetic wave can be radiated from it and propagate in the free space between the monopole and CGC, the current is then induced on the graphene of CGC, and finally the radiated wave spreads across the free space outside the CGC. Therefore, the proposed antenna can be seen as a TL model with four cascaded networks, as shown in Fig. 3.

The transmission line (its length and characteristic admittance are d and $Y_0 = 1/120\pi$ S, respectively) in section (ii) is the equivalence of the free space between the monopole and the coating, Y_{mp} in section (i) represents the admittance of the monopole, and Y_g in section (iii) and Y_L in section (iv) represent the admittances of graphene and the outer free space, respectively. The Y_{mp} is mainly determined by the length l of the monopole, and then it can be used to obtain the inherent resonant frequency f_0 (or the inherent resonant wavelength λ_0) of the monopole. For $l = 4.5$ mm, f_0 is approximately equal to

15 GHz, that is, $l \approx 0.225\lambda_0$.

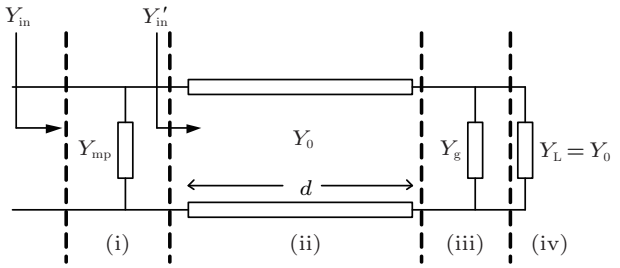


Fig. 3. The TL model of the antenna.

The *ABCD* matrices for sections (ii) and (iii) are expressed as

$$\begin{bmatrix} A & B \\ C & D \end{bmatrix}_{\mathrm{II}} = \begin{bmatrix} \cosh(\mathrm{j}\beta_n d) & \dfrac{\sinh(\mathrm{j}\beta_n d)}{Y_0} \\ Y_0 \sinh(\mathrm{j}\beta_n d) & \cosh(\mathrm{j}\beta_n d) \end{bmatrix}, \tag{5}$$

$$\begin{bmatrix} A & B \\ C & D \end{bmatrix}_{\mathrm{iii}} = \begin{bmatrix} 1 & 0 \\ Y_g & 1 \end{bmatrix}. \tag{6}$$

Then, the chain transmission matrix of the above two sections is derived as

$$\begin{bmatrix} A & B \\ C & D \end{bmatrix} = \begin{bmatrix} \cosh(\mathrm{j}\beta_n d) + Y_g/Y_0 \sinh(\mathrm{j}\beta_n d) & \sinh(\mathrm{j}\beta_n d)/Y_0 \\ Y_0 \sinh(\mathrm{j}\beta_n d) + Y_g \cosh(\mathrm{j}\beta_n d) & \cosh(\mathrm{j}\beta_n d) \end{bmatrix}. \tag{7}$$

Therefore, the input admittance of Y'_{in} in Fig. 3 can be written as

$$Y'_{in} = \frac{C/Y_L + D}{A/Y_L + B} = Y'_{in,Re} + jY'_{in,Im}, \tag{8}$$

where

$$Y'_{in,Re} = \frac{Y_0^2 (Y_g + Y_0) \sec^2(\beta_n d)}{Y_0^2 + (Y_g + Y_0)^2 \tan^2(\beta_n d)},$$

$$Y'_{in,Im} = -\frac{Y_0 Y_g (Y_g + 2Y_0) \tan(\beta_n d)}{Y_0^2 + (Y_g + Y_0)^2 \tan^2(\beta_n d)}.$$

From Fig. 1, Y_g in the microwave region can be considered as real numbers. The cascaded networks (ii), (iii), and (iv) illustrate the coupling relationship between the monopole and the graphene-based coating. From Eq. (8), it can be derived that there are a serial of coupling resonances when $Y'_{in,Im} = 0$ (i.e. $\tan(\beta_n d) = 0$), and then the corresponding coupling frequencies may be determined as

$$f_n = \frac{n}{2}\frac{c_0}{d}, \quad (n = 1, 2, 3, \ldots), \tag{9}$$

where c_0 is the speed of the electromagnetic wave in the free space, and n is the order of the coupling frequency. The f_1 corresponds to the first-order or major coupling frequency, while the other f_n denotes the high-order coupling frequency. From Eq. (9), we can see that the coupling frequencies vary as a function of the radius d of the CGC.

To investigate the influence of radius d on the impedance bandwidth of the proposed antenna, we simulate the reflection coefficient using commercial software CST Microwave Studio with all the surface impedances of the 36 subdomains of graphene (see Fig. 2(a)) being 300 Ω, as shown in Fig. 4(a).

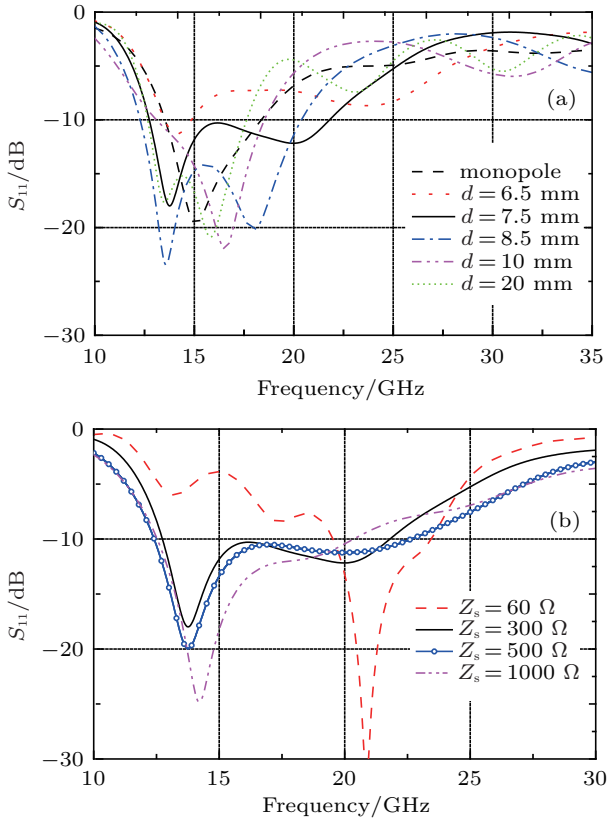


Fig. 4. (color online) Simulated S_{11}. (a) The monopole and the proposed antenna for different d. (b) The proposed antenna for different Z_s.

Figure 4 shows that there are many resonant frequencies, where the first frequency (f_0) is mainly determined by the length of the monopole and the others (f_n, $n = 1, 2, 3, \ldots$) are caused by the coupling resonance of the monopole and the CGC. These coupling frequencies can also be obtained from Eq. (9). In order to validate it, we compare the coupling frequencies calculated by Eq. (9) with those extracted from the simulations (see Fig. 4(a)), as listed in Table 1, where $f_{n-\mathrm{tlm}}$ and $f_{n-\mathrm{cst}}$ are the coupling frequencies obtained from Eq. (9) and CST, respectively. It is obvious that the coupling frequencies calculated from Eq. (9) agree well with those simulated by CST, and then the accuracy and the effectiveness of the above analysis are validated. In Table 1, $f_{2-\mathrm{cst}}$ for $d \leq 8.5$ mm and $f_{3-\mathrm{cst}}$ for $d \leq 10$ mm are higher than 35 GHz, thus they are not exhibited in Fig. 4(a); $f_{3-\mathrm{cst}}$ for $d \leq 8.5$ mm are not listed because they are very inconspicuous in the simulated results; $f_{1-\mathrm{cst}}$ for $d \geq 10$ mm are also not listed because it is drowned in the inherent resonance. By optimizing the coupling resonance of the antenna, the multiple resonance frequencies can be brought closer,[29–32] and the ultra-wideband

Table 1. Coupling frequencies (GHz) and the relative error (%) simulated by TL method and CST for different d (mm).

d	$f_{1-\mathrm{tlm}}$	$f_{1-\mathrm{cst}}$	Error	$f_{2-\mathrm{tlm}}$	$f_{2-\mathrm{cst}}$	Error	$f_{3-\mathrm{tlm}}$	$f_{3-\mathrm{cst}}$	Error
6.5	23.1	23.3	0.87	46.2	45.6	1.30	69.2	–	–
7.5	20.0	20.0	0.00	40.0	40.5	1.25	60.0	–	–
8.5	17.7	18.0	1.70	35.3	36.1	2.27	53.0	–	–
10	15.0	–	–	30.0	31.0	3.33	45.0	46.1	2.44
20	7.5	–	–	15.0	15.8	5.33	22.5	23.0	2.22

impedance characteristic is then obtained. Figure 4(a) shows that an ultra-bandwidth of 52.5% is realized when $d = 7.5$ mm.

Moreover, when all of the surface impedances of the 36 subdomains of graphene have the same value and the values are 60 Ω, 300 Ω, 500 Ω, and 1 kΩ, respectively, the reflection coefficients of the proposed antenna are displayed in Fig. 4(b), which shows that the widest relative bandwidth increases to 58.5% when Z_s equals to 500 Ω. This implies that the graphene with 500 Ω matches the monopole to free space better.[33]

The above investigations are based on the same impedances; namely, the impedance of LIS is equal to that of HIS for each subdomain of graphene. For example, for four curves in Fig. 4(b), the impedance of each subdomain is equivalent to 60 Ω, 300 Ω, 500 Ω, and 1 kΩ, respectively. In order to further study the influence of the surface impedance on the performance of the proposed antenna, we define R_{LIS}–R_{HIS} as the different impedance counterpart of LIS and HIS, that is the LIS and HIS having different impedances. Here, the LIS and HIS are coded by $\underbrace{1\ldots1}_{18}\underbrace{0\ldots0}_{18}$ (see Fig. 2(c)), and R_{LIS}–R_{HIS} are respectively 5–377 Ω, 5–1000 Ω, 5–5000 Ω, 50–5000 Ω, and 377–5000 Ω, we simulate the reflection coefficients for these five cases, as shown in Fig. 5(a). We can clearly see that R_{LIS}–R_{HIS} has great influence on the bandwidth of the antenna. When R_{LIS}–R_{HIS} is 5–5000 Ω, the antenna occupies the greatest bandwidth. On the other hand, the coupling resonance becomes stronger and stronger with the decrease of R_{LIS}–R_{HIS}, which means that the metallicity of the graphene is more obviously.

For the given R_{LIS}–R_{HIS}, such as 5–5000 Ω, the different binary codes of LIS and HIS may affect the impedance bandwidth of the proposed antenna. To verify this, we take binary codes of $\underbrace{1\ldots1}_{5}\underbrace{0\ldots0}_{31}$, $\underbrace{1\ldots1}_{14}\underbrace{0\ldots0}_{22}$, $\underbrace{1\ldots1}_{18}\underbrace{0\ldots0}_{18}$, $\underbrace{1\ldots1}_{22}\underbrace{0\ldots0}_{14}$, $\underbrace{1\ldots1}_{27}\underbrace{0\ldots0}_{9}$, and as examples to simulate the reflection coefficient, as shown in Fig. 5(b). We observe that there are two resonances, which correspond to the inherent resonance and the first-order coupling resonance, and the two resonances are influenced by the subdomain number of LIS. In detail, the coupling resonance becomes strong whereas the inherent resonance becomes weak with the increase of the subdomain number of LIS. Because of its multiple resonance characteristic, the proposed antenna can operate in ultra-wideband by optimizing the geometric parameter.[31] It is worthy to note that, in this design, the optimized relative bandwidth of 67% is achieved for the binary code of $\underbrace{1\ldots1}_{18}\underbrace{0\ldots0}_{18}$ and LIS–HIS of 5–5000 Ω.

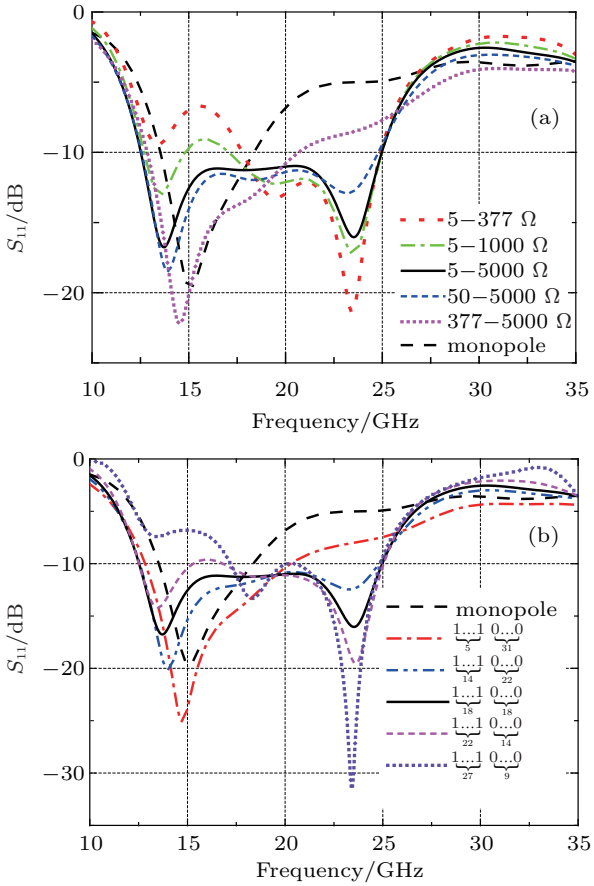


Fig. 5. (color online) The S_{11} of the monopole and the proposed antenna surrounded by the CGC with (a) the same binary code and (b) different binary.

3.2. Pattern reconfiguration characteristics of the proposed ultra-wideband antenna

As described above, the graphene acts as a metallic plate for the lower impedance, this is used to control the radiation pattern of the antenna. Fortunately, the size and position of the metallic plate can be modified by controlling the biased voltage $V_{\mathrm{DC}i}$, which results in the tunability of the radiation pattern of the antenna. In order to demonstrate this, we set R_{LIS}–R_{HIS} as 5–5000 Ω and simulate the radiation patterns for different binary codes of LIS and HIS, as shown in Figs. 6 and 7. From Fig. 6(a), we can see that when the code is set as $\underbrace{0\ldots0}_{36}$ (namely all the surface impedances of the 36 subdomains are 5000 Ω),

the antenna is omnidirectional with the gain of 2.81 dB, corresponding to the radiation of the monopole. However, for the other codes as shown in Figs. 6(b)–6(d), the antenna gives directional radiation and its directivity is changed when the code is altered, implying tunability of radiation pattern. Furthermore, we also observe that the elevation angles of the main lobe vary between 20° and 30° in the whole frequency range (see Fig. 7), showing perfect radiation performance.

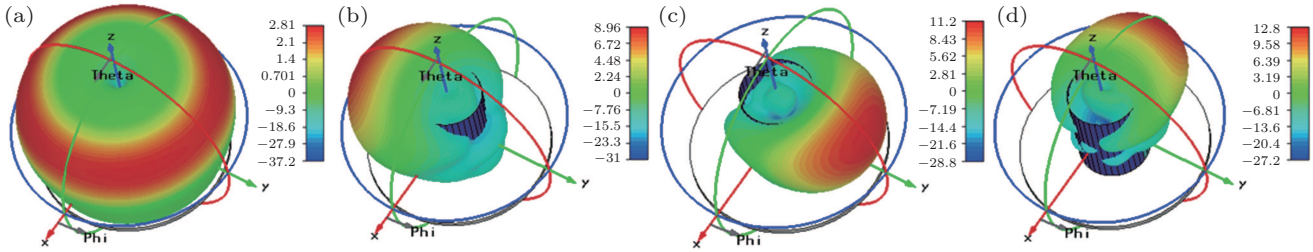


Fig. 6. 3D radiation pattern under the conditions of (a) $\underbrace{0\ldots0}_{36}$ at 14 GHz, (b) $\underbrace{1\ldots1}_{18}\underbrace{0\ldots0}_{18}$ at 14 GHz, (c) $\underbrace{0\ldots0}_{18}\underbrace{1\ldots1}_{18}$ at 18 GHz, and (d) $\underbrace{1\ldots1}_{9}\underbrace{0\ldots0}_{18}\underbrace{1\ldots1}_{9}$ at 22 GHz.

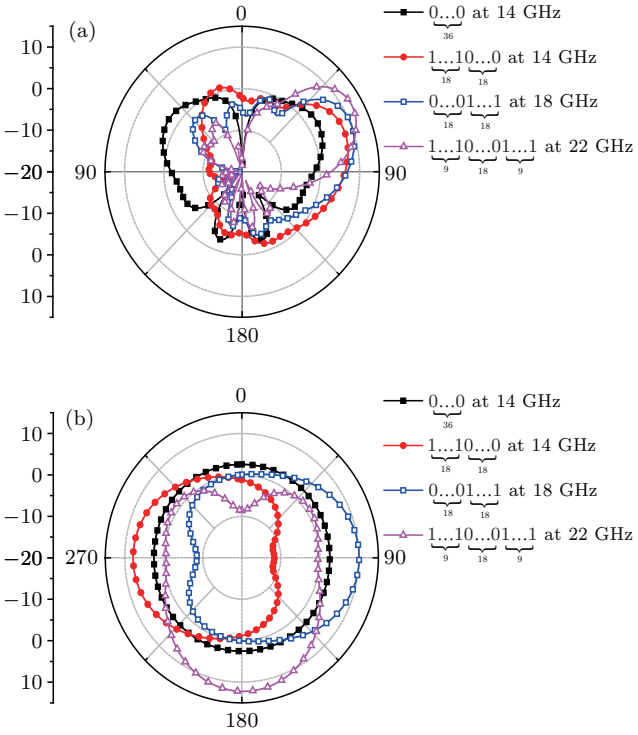


Fig. 7. The (a) *E*-plane and (b) *H*-plane radiation patterns along the main beam corresponding to Fig. 6.

In order to further investigate the radiation performance of the antenna, we simulate the *H*-plane half-power beam (HPBW) for different numbers of the LIS subdomains, as shown in Fig. 8. When the number of the LIS subdomains is 18, 12, and 6, the HPBW is 79.1°, 97.9°, and 151.5°, respectively, which implies that the *H*-plane HPBW of the antenna increases with the reduction of the number of the LIS subdomains. Actually, the increment of the number of the LIS subdomains is to enlarge the size of the metallic plate, and hence the HPBW can be effectively reduced. Therefore, it is convenient to control the HPBW of the antenna by changing the number of the LIS subdomains.

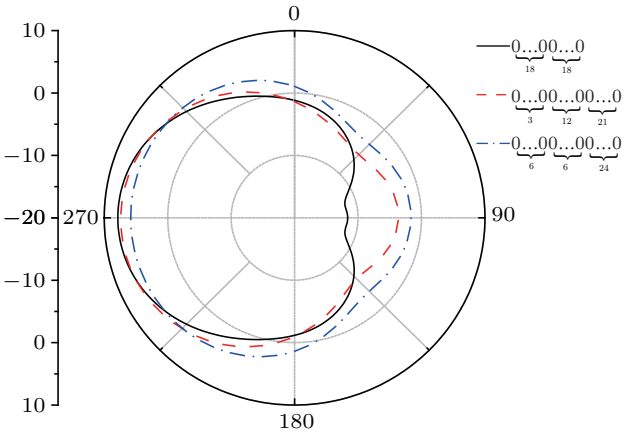


Fig. 8. The *H*-Plane radiation patterns with different numbers of LIS subdomains at 14 GHz.

4. Conclusion

We have proposed an ultra-wideband pattern reconfigurable antenna with graphene-based coating in microwave region. The antenna is a coaxial hollow dielectric monopole coated by a cylindrical graphene-based impedance surface. A transmission line method has been used to validate the ultra-wideband impedance characteristic. By changing the bias voltages applied to the graphene, the proposed antenna can work in the directional mode orienting in arbitrary azimuth or omnidirectional mode. Furthermore, the gain of the proposed antenna increases compared to that of the monopole without the graphene coating. The pattern reconfiguration and the optimized relative bandwidths of 67% (for directional mode) and 58.5% (for omnidirectional mode) are obtained, which extends the applications of the proposed antenna significantly.

References

[1] Geim A K and Novoselov K S 2007 *Nat. Mater.* **6** 183
[2] Lee C, Wei X, Kysar J W and Hone J 2008 *Science* **321** 385
[3] Novoselov K S, Falko V I, Colombo L, Gellert P R, Schwab M G and Kim K 2012 *Nature* **490** 192

[4] Nair R R, Blake P, Grigorenko A N, Novoselov K S, Booth T J, Stauber T, Peres N M R and Geim A K 2008 *Science* **320** 1308

[5] Kim K S, Zhao Y, Jang H, Lee S Y, Kim J M, Kim K S, Ahn J H, Kim P, Choi J Y and Hong B H 2009 *Nature* **45** 7706

[6] Eda G, Fanchini G and Chhowalla M 2008 *Nat. Nanotechnol.* **3** 270

[7] Murali R, Brenner K, Yang Y, Beck T and Meindl J D 2009 *IEEE Electron Device Lett.* **30** 611

[8] Vakil A and Engheta N 2011 *Science* **332** 1291

[9] Grigorenko A N, Polini M and Novoselov K S 2012 *Nat. Photon.* **6** 749

[10] Chen P Y, Argyropoulos C and Alu A 2013 *IEEE Transactions on Antennas and Propagation* **61** 1528

[11] He S and Chen T 2013 *IEEE Transactions on Terahertz Science and Technology* **3** 757

[12] Xu B Z, Gu C Q, Li Z, Liu L L and Niu Z Y 2014 *IEEE Antennas and Wireless Propagation Letters* **13** 822

[13] Jiang Y N, Wang Y, Ge D B, Li S M, Cao W P, Gao X and Yu X H 2016 *Acta Phys. Sin.* **65** 054101 (in Chinese)

[14] Aldrigo M, Dragoman M, Costanzo A and Dragoman D 2014 *J. Appl. Phys.* **116** 114302

[15] Wang X C, ZhaoW S, Hu J and Yin W Y 2015 *IEEE Transactions on Nanotechnology* **14** 62

[16] Esquius-Morote M, Gomez-Diaz J S and Perruisseau-Carrier J 2014 *IEEE Transactions on Terahertz Science and Technology* **4** 116

[17] Carrasco E and Perruisseau-Carrier J 2013 *IEEE Antennas and Wireless Propagation Letters* **12** 253

[18] Chen X H, Yao Y, Qu S W, Wu Y S and Chen X D 2016 *Electronics Letters* **52** 494

[19] Anand S T, Mayur S D and Sriram K D 2015 *Physica E* **66** 67

[20] Rajni B and Anupma M 2016 *Optik* **127** 2089

[21] Skulason H S, Nguyen H V, Guermoune A, Sridharan V, Siaj M, Caloz C and Szkopek T 2011 *Appl. Phys. Lett.* **99** 153504

[22] Dragoman M, Neculoiu D, Cismaru A, Muller A A, Deligeorgis G, Konstantinidis G, Plana R and Dragoman D 2011 *Appl. Phys. Lett.* **99** 033112

[23] Huang Y, Wu L S, Tang M and Mao J 2012 *IEEE Transactions on Nanotechnology* **11** 836

[24] Tamagnone M, Gomez-Diaz J S, Mosig J and Perruisseau-Carrier J 2013 *IEEE MTT-S International Microwave Symposium digest (IMS)*, June 2–7, 2013, Seattle, USA, p. 1

[25] Bae S, Kim H, Lee Y, Xu X, Park J S, Zheng Y, Balakrishnan J, Lei T, Kim H R, Song Y I, Kim Y J, Kim K S, Ozyilmaz B, Ahn J H, Hong B H and Iijima S 2010 *Nat. Nanotechnol.* **5** 574

[26] Zaretski A V , Moetazedi H, Kong C, Sawyer E J, Savagatrup S, Valle E, O'Connor T F, Printz A D and Lipomi D J 2015 *Nanotechnology* **26** 045301

[27] Hanson G W 2008 *J. Appl. Phys.* **103** 064302

[28] Gusynin V P, Sharapov S G and Carbotte J P 2007 *J. Phys.: Condens. Matter* **19** 026222

[29] Lu J H and Yeh C H 2012 *IEEE Transactions on Antenna and Propagation* **60** 3091

[30] Tuovinen T and Berg M 2014 *Progress in Electromagnetics Research* **144** 249

[31] Gao X, Han X, Cao W P, Li H O, Ma H F and Cui T J 2015 *IEEE Transactions on Antenna and Propagation* **63** 3522

[32] Jiang Y N, Zhang W C, Wang J, Cao W P and Lin Y Y 2016 *Eur. Phys. J. Appl. Phys.* **73** 11301

[33] Ziolkowski R W and Kipple A D 2003 *IEEE Transactions on Antenna and Propagation* **51** 2626